Raman scattering of phonon-plasmon coupled modes in self-assembled GaN nanowires

K. Jeganathan, R. K. Debnath, R. Meijers, T. Stoica, R. Calarco, D. Grützmacher, and H. Lüth

Citation: Journal of Applied Physics **105**, 123707 (2009);
View online: https://doi.org/10.1063/1.3148862
View Table of Contents: http://aip.scitation.org/toc/jap/105/12
Published by the American Institute of Physics

Raman scattering of phonon-plasmon coupled modes in self-assembled GaN nanowires

K. Jeganathan,[1,2,a)] R. K. Debnath,[1] R. Meijers,[1] T. Stoica,[1] R. Calarco,[1] D. Grützmacher,[1] and H. Lüth[1]

[1]*Institute of Bio-and Nanosystems (IBN-1) and Center of Nanoelectronic Systems for Information Technology (CNI), Research Centre Jülich GmbH, D-52425 Jülich, Germany*

[2]*Centre for Nanoscience and Nanotechnology, Bharathidasan University, Tiruchirappalli, 620 024, India*

(Received 5 February 2009; accepted 9 May 2009; published online 22 June 2009)

We report the determination of free-electron concentration and mobility of free-standing GaN nanowires (NWs) by line shape analysis of the coupled longitudinal optical phonon-plasmon Raman modes ($L+$). The E_2^{high} phonon mode at 566.9 cm^{-1} with a sharp linewidth of 2.8 cm^{-1} indicates strain free NWs with high crystalline perfection. The lattice temperature of the NWs was varied between 313 and 472 K by varying the excitation laser beam power. For unintentionally doped samples at room temperature, an average electron concentration and mobility of strain free NWs were found to be $\sim 2\times 10^{17}$ cm^{-3} and 460 $\text{cm}^2/\text{V s}$, respectively. We have shown that the electron concentration does not change significantly over a temperature range between 313 and 472 K. The electron mobility decreases at high temperatures, in agreement with literature data for compact layers. For Si-doped NWs, the $L+$ phonon peak is strongly upshifted indicating a higher free-carrier concentration of about 1×10^{18} cm^{-3}. Asymmetric broadening observed at the lower frequency side of the $L+$ phonon peak might be ascribed to the enhancement in surface optical modes due to the high surface-to-volume ratio of NWs. © *2009 American Institute of Physics*.
[DOI: 10.1063/1.3148862]

I. INTRODUCTION

Semiconductor nanowires (NWs) are emerging as powerful building blocks for future nanodevices such as light emitting diodes,[1–3] laser diodes,[4,5] photodetectors,[6,7] chemical and biochemical sensors,[8,9] and high-temperature and high-power electronic devices[10,11] because of their inherent interesting material properties. A remarkable progress has been made both in the synthesis of GaN-related NWs[12–15] and device process technologies.[5,11,16] However, some of the basic properties of the NWs including electrical properties, lattice dynamics, and surface optical (SO) modes remain poorly investigated. Measurement methods for the electronic transport properties of GaN NWs are needed to facilitate the design and modeling of NW-based devices. Transport studies are typically performed by Hall-bar contact schemes to derive free-electron concentration and mobilities. A cumbersome and labor intensive electron-beam lithography process is often used to fabricate metal contacts on NWs for electrical studies.[17] However, Hall-effect measurements of test structures fabricated by this process have not yet been reported. On the other hand, Raman scattering provides a fast contactless and nondestructive method to determine the electrical parameters on an area spatially defined by the focal size of the optical beam.[18,19] Further information on the interaction of the free-electron plasmon with phonons, optical surface phonon modes, strain, and crystalline quality of NWs can be obtained simultaneously using the Raman technique.

In doped polar semiconductors with significant free carrier concentration, the longitudinal optical (LO) phonons strongly interact with free-carrier plasmons through electric fields, which produce two coupled LO phonon-plasmon modes, denoted by $L+$ and $L-$. The character of these modes highly depends on the plasmon frequency (ω_p). When ω_p is lower than the uncoupled LO phonon frequency, the $L-$ mode behaves like a plasmon, whereas the $L+$ mode is phononlike. The frequency of the $L+$ mode increases with an increase in carrier concentration, and, at high carrier concentration, the character of the $L+$ mode changes from phononlike to plasmonlike.[19–21]

In unintentionally low doped GaN, the $L+$ mode is found at higher frequency from the LO phonon due to the strong coupling with plasmons. The $L+$ mode shifts further to higher frequency and broadens with increasing carrier concentration. This behavior was exploited in order to evaluate the doping carrier concentration by an empirical formula[22]

$$n = 1.1\times 10^{17}(\omega_{L+}-\omega_{\text{LO}})^{0.764} \quad (\text{valid for } n < 1\times 10^{19}\ \text{cm}^{-3}) \tag{1}$$

where, n is the carrier concentration, ω_{L+} is the frequency of the $L+$ mode, and ω_{LO} is the frequency of the uncoupled LO phonon ($\omega_{\text{LO}}=735$ cm^{-1}). For a precise evaluation of carrier concentration and mobility by Raman scattering, a line shape analysis based on the carrier scattering deformation-potential mechanism should be employed.[19–21] The carrier densities evaluated from Hall measurements have been reported to be in good agreement with the calculated values by line shape analysis.[19] A previous study on the electronic properties of GaN nanostructures by line shape analysis was based on a bundle of as-grown vertically aligned NWs.[17] However, the phonon-plasmon approach has not been applied to evaluate

a)Electronic mail: kjeganathan@yahoo.com.

the electronic properties of free-standing NWs (FSNWs) as a function of lattice temperature. The aim of this article is a detailed line shape analysis of μ-Raman scattering spectra recorded in the backscattering configuration under various excitation laser power to elucidate the intrinsic properties of free-standing GaN NWs (free-electron concentration and mobility) as a function of lattice temperature.

II. EXPERIMENT

Self-assembled GaN NWs were fabricated by plasma-assisted molecular beam epitaxy on Si (111) substrates under nitrogen rich ($Ga/N \ll 1$) growth conditions at 780 °C, which leads to the desired columnar growth in *c*-direction. Details of the fabrication process can be found elsewhere.[12] The GaN NWs were also nominally doped with Si impurity atoms ($F_{Si}=1.0\times10^{-9}$ mbar) under identical growth parameters used for undoped GaN NWs [$F_{Ga}=3.0\times10^{-8}$ mbar, rf-power $P_{rf}=500$ W, and nitrogen flow rate of 5 SCCM (SCCM denotes standard cubic centimeter per minute)]. The diameter and density of the Si doped as-grown GaN NWs is much less than that of undoped counterpart. The Si found to act as an antisurfactant in GaN growth which reduces the adatoms mobilities resulting in well isolated GaN NWs with the diameter $\sim 70 \pm 20$ nm. FSNWs with an average diameter of $\sim 125 \pm 25$ nm was suspended on a glass template by removing them from their original substrate. It is considered that the *c*-axis NW lies along the *x*-axis with respect to the template's surface. μ-Raman scattering measurements were performed in backscattering geometry with a spectral resolution of 0.3 cm^{-1}. A wavelength of the 514.5 nm of an Ar-ion laser was used as excitation source and the laser beam was focused through a microscope (100×, numerical aperture of 0.9) to a spot size of about 1 μm in diameter. A liquid nitrogen cooled charge coupled device was used to collect the scattered signal (1800 grooves/mm grating). In order to study the behavior of phonons, the laser power dependent Raman spectra were recorded between 0.25 to 3.65 mW excitation powers.

III. RESULTS AND DISCUSSIONS

A typical cross-sectional field emission scanning electron microscope micrograph of GaN NWs is shown in the inset of Fig. 1. An assembly of NWs which are well separated and quite homogenous in length and diameter distribution can easily be achieved by optimizing the growth parameters.

Group theory predicts four Raman active modes at the Γ-point of the Brillouin zone of hexagonal GaN: A_1, E_1, E_2^{high}, and E_2^{low}.[19] Since A_1 and E_1 are polar modes, they split into two components due to the interaction by long range Coulomb fields which leads to energy differences between phonons polarized longitudinally (LO) and transversely (TO) to the direction of propagation of the phonons. Figure 1 shows a Raman spectrum of GaN FSNW measured in quasibackscattering geometry for a laser power of 0.25 mW. Forbidden optical modes are also present in Fig. 1 they can be related to morphic quasimodes, which appeared due to symmetry violation of crystal axes orientation. If the NWs

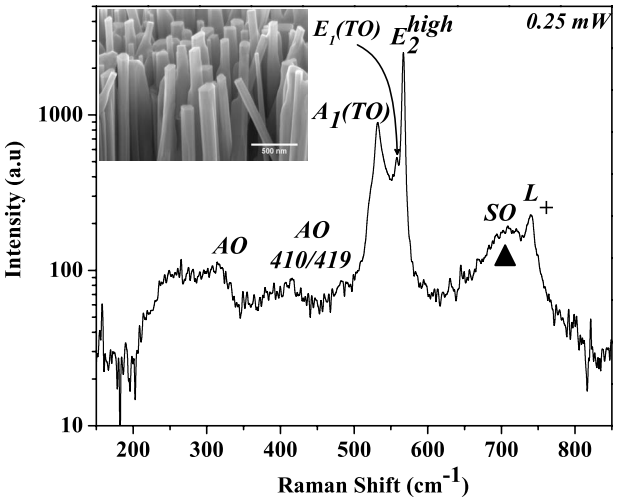

FIG. 1. Micro-Raman spectra of a free-standing GaN NW recorded in quasibackscattering geometry for excitation laser power of 0.25 mW near the sample surface. The inset shows a cross-sectional SEM image of as-grown GaN NWs on Si (111) substrate.

are tilted relative to the laser excitation direction, then the scattered signal from the wire are not at the crystal-symmetry axes. The A_1 (TO) and E_2^{high} mode frequencies are found at 533.1 and 566.9 cm^{-1}, respectively, and they are consistent with strain free values from literature.[19] The A_1 and E_1 are polar modes in which long range electrostatic forces govern over crystalline anisotropy, under this circumstance the intermixing of A_1 and E_1 modes can easily be identified from the A_1-E_1 splitting. The observed E_1(TO)-A_1(TO) splitting in the NWs of 25 cm^{-1} is slightly smaller than the E_1(TO)-A_1(TO) splitting of 27 to 29 cm^{-1} for bulk GaN, as reported in the literature.[19,23–27] From the similarity of the E_1(TO)-A_1(TO) splitting in the NWs to the E_1(TO)-A_1(TO) splitting in bulk GaN, it can be concluded that intermixing between the A_1 and E_1 modes in NWs is small. The violation of Raman selection rules in the backscattering geometry for NWs cannot be intimately related to the intermixing of phonon modes. Thus, it can be concluded that the observed *L*+ mode is purely due to LO phonons of A_1 symmetry. A full width at half maximum (FWHM) of the sharp E_2^{high} mode of 2.8 cm^{-1} exhibits a good crystalline quality of strain-free FSNWs. The coupled mode of *L*+ is observed at 739.4 cm^{-1}. The theoretical frequency of the *L*− mode for the given plasmon frequency (136 cm^{-1}) corresponding to the *L*+ mode is at 98 cm^{-1}.[28] Due to the superposition with the Rayleigh tail below 100 cm^{-1}, this mode is not clearly resolved in our NWs. Thus only the *L*+ mode has been used for the line shape analysis.

Figure 1 also shows a broad asymmetric peak centered around 703.1 cm^{-1} at the lower frequency side of the *L*+ phonon mode. It might be assigned to a SO mode which is normally absent in bulk compact GaN films.[29] The origin of the SO mode can be tentatively attributed to the high surface-to-volume ratio and the broken longitudinal symmetry at the surface of NWs. Table I shows the phonon frequencies and symmetries of the strongest modes observed in the first-order Raman spectra of hexagonal GaN NWs for the excitation laser power of 0.25 mW (31.8 kW/cm^2). The

TABLE I. Typical phonon frequencies and symmetries (for 0.25 mW) observed by Raman scattering for free-standing hexagonal GaN NWs.

Frequency (cm^{-1})		
FS-GaN NW	GaN bulk	Symmetry
311–316	317	A_1: acoustic overtone[a]
410	410	A_1: acoustic overtone[a]
419	420	A_1 and E_1: acoustic overtones[a]
533.1	532.6 ± 2.3 [b]	A_1(TO)
558	560 ± 3.1 [b]	E_1(TO)
566.9	566.2[b]	E_2^{high}
703.1	⋯	SO: surface optical mode
739.4	735 ± 1.6 [b]	A_1(LO)/$L+$

[a]See Ref. 23.
[b]See Refs. 19 and 23–27.

strain free values of GaN are also tabulated for comparison. The Raman scattering on FSNWs is preferable because it provides well resolved phonon peaks and also excludes the influence of Si substrate in the spectrum. The A_1(TO) phonon frequency is about 533 cm^{-1} which is always superimposed with the long tail of Si substrate peak as it has intense broad phonon peak at 520 cm^{-1}.

As the NWs were suspended on the insulating glass plates which have poor thermal contact, the NWs are easily heated during laser irradiation. The experimentally recorded maximum intensities (E_2^{high}) of stokes and weak anti-Stokes lines, and Lorentzian fitted peak position of E_2^{high} stokes have been used for the determination of laser induced lattice temperature. The temperature rise of the NWs due to laser induced lattice heating at various excitation laser power (0.25 to 3.65 mW) was determined from the intensity ratio of the E_2^{high} Stokes peak to corresponding anti-Stokes peak[30]

$$\frac{I_S}{I_{AS}} \propto \exp(\hbar\omega_{E_2}/k_B T), \tag{2}$$

where I_S is the intensity of E_2^{high} Stokes, I_{AS} is the intensity of E_2^{high} anti-Stokes, k_B is the Boltzmann constant, and $\hbar = h/2\pi$ where h is Planck's constant. The estimated local temperature (hereafter it is referred to as lattice temperature) is ~313 K for the excitation laser power of 0.25 mW. The laser induced lattice temperature increases linearly with the increase in excitation power. Figures 2(a) and 2(b) show the corresponding E_2^{high} and A_1(LO) phonon shift, respectively, as a function of excitation power. The phonons shift to lower frequency and the integrated intensity increases with the increase in laser power. The frequency of the E_2^{high} mode shifts from 566.9 to 566.3 cm^{-1} (redshift of 0.6 cm^{-1}) when the excitation power increased from 0.25 to 3.65 mW. Additionally the coupled mode substantially shifts from 739.4 cm^{-1} to lower frequency by about 1.0 cm^{-1}. The plausible explanation for the redshift is the lattice temperature rise in NWs due to the laser irradiation. Figures 3(a) and 3(b) show the FWHM and peak positions of E_2^{high} and $L+$ phonon as a function of lattice temperature. Although the change in E_2^{high} peak width is marginal as a function of temperature, the $L+$ mode is over damped with the plasmon. Further, it can easily be observed that the E_2^{high} and $L+$ phonons linewidth increases and that the Raman frequency shift decreases with an increase in lattice temperature.

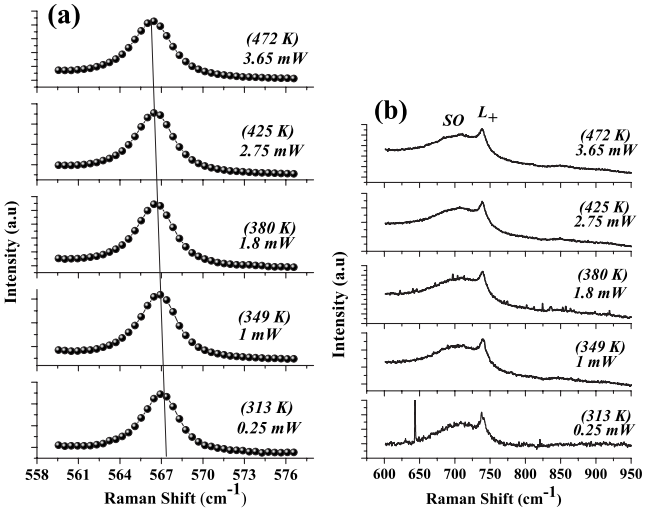

FIG. 2. Laser power dependent Raman spectra of GaN NW (a) Raman shift of the E_2^{high} phonon mode and (b) coupled LO phonon-plasmon mode.

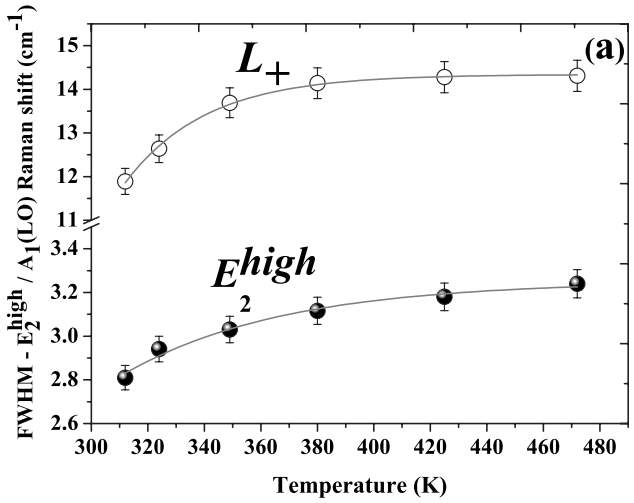

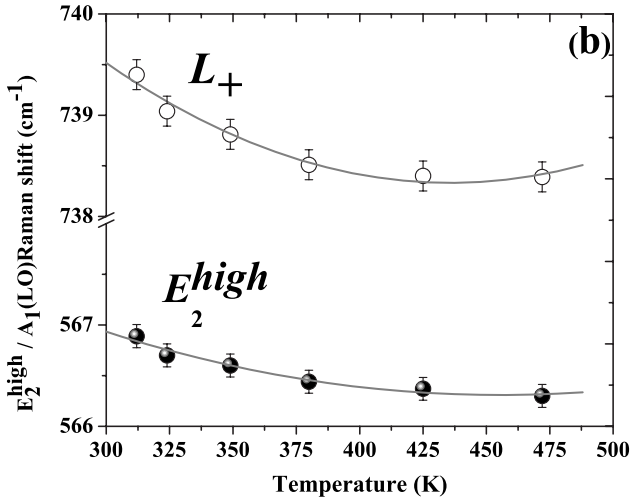

FIG. 3. Linewidth and peak positions of E_2^{high} and $L+$ modes as a function of lattice temperature. (a) FWHM of E_2^{high} and $L+$ modes and (b) peak position of E_2^{high} and $L+$ modes.

The Raman intensity profile of a coupled $L+$ mode for hexagonal crystals can be expressed[21,31] as

$$I_A = SA(\omega)\mathrm{Im}\left[-\frac{1}{\varepsilon(\omega)}\right], \tag{3}$$

where ω is the Raman frequency, S is a proportionality constant, and $\varepsilon(\omega)$ is the dielectric function. The parameter $A(\omega)$ is given by[31]

$$\begin{aligned} A(\omega) = 1 + 2C\omega_T^2[&\omega_p^2\gamma(\omega_T^2 - \omega_{L+}^2) \\ &- \omega_{L+}^2\Gamma(\omega_{L+}^2 + \gamma^2 - \omega_p^2)]/\Delta \\ &+ (C^2\omega_T^4/\Delta)\{\omega_p^2[\gamma(\omega_L^2 - \omega_T^2) + \Gamma(\omega_p^2 - 2\omega_{L+}^2)] \\ &+ \omega_{L+}^2\Gamma(\omega_{L+}^2 + \gamma^2\ \}/(\omega_L^2 - \omega_T^2), \end{aligned} \tag{4}$$

$$\begin{aligned} \Delta = \omega_p^2\gamma[&(\omega_T^2 - \omega_{L+}^2)^2 + (\omega_{L+}\Gamma)^2] \\ &+ \omega_{L+}^2\Gamma(\omega_L^2 - \omega_T^2)(\omega_{L+}^2 + \gamma^2), \end{aligned} \tag{5}$$

where, ω_T and ω_L are the unstrained TO- and LO-phonon frequencies, respectively, and γ and Γ (FWHM of peak) are the plasmon and phonon damping constants, respectively. C is Faust–Henry coefficient which determines the ratio of scattering by TO and LO phonons in an undoped GaN crystal.[31] ω_p is the plasmon frequency and ω_{L+} is the frequency of coupled mode. The dielectric function $\varepsilon(\omega)$ is given by the contribution of plasmon and phonon

$$\begin{aligned} \varepsilon(\omega) = \varepsilon_\infty[&1 + (\omega_L^2 - \omega_T^2)/(\omega_T^2 - \omega_{L+}^2 - i\omega\Gamma) \\ &- \omega_p^2/(\omega_{L+}^2 + i\omega_{L+}\gamma)]. \end{aligned} \tag{6}$$

The line shape of the coupled mode $L+$ can be fitted with the function given in Eq. (3). $\varepsilon(\omega)$ and $A(\omega)$ are functions of the plasmon damping constant (γ), phonon damping (Γ), and plasmon frequency (ω_p). The proportionality constant S is reasonably treated as independent of carrier concentration. The precise fitting of the line shape is quite important for the unique determination of the fitting parameters γ, Γ, and ω_p. The strain free values of $A_1(\mathrm{TO})=533\ \mathrm{cm}^{-1}$ and the uncoupled $A_1(\mathrm{LO})=735\ \mathrm{cm}^{-1}$ are used as constants for fitting. Careful attention has been paid to the baseline correction of the experimental data and the deconvolution of the asymmetric low frequency peak denoted as SO mode in Fig. 1. The inset of Fig. 4 shows a typical line shape of the experimental (open circle) and the theoretical fitted curve (gray line) of the phonon-plasmon coupled $L+$ mode. The reproducible fitting parameters γ, Γ, and ω_p have been obtained from the above line shape analysis. They can be related to the free-carrier concentration (n) and effective electron mass ($m^*=0.2m_e$) (Refs. 19 and 20) by

$$\omega_p^2 = \frac{\pi n e^2}{\varepsilon_\infty m^*}, \tag{7}$$

and

$$\gamma = \frac{e}{m^*\mu} \tag{8}$$

The electron concentration (n) and mobility (μ) are obtained by a line shape analysis of the coupled mode $L+$ recorded at

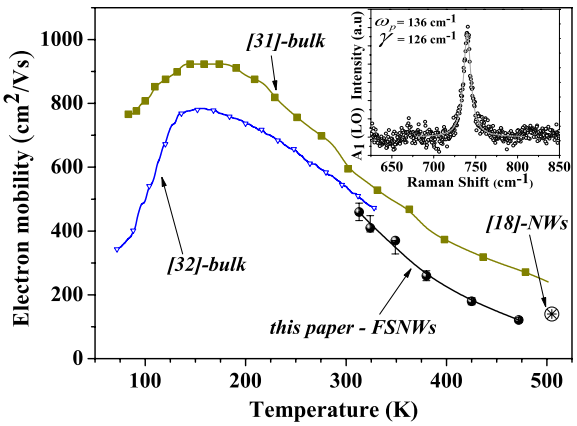

FIG. 4. (Color online) The electron mobility as a function of laser induced temperature in comparison with data extracted from literature for GaN bulk [31,32] and NWs [18]. The inset shows Raman spectrum of coupled LO phonon-plasmon mode ($L+$) of free-standing GaN NWs for 1 mW (the gray line is the fitting curve by line shape analysis and open circle is the experimental curve).

0.25 mW excitation laser power to be $2.2\times10^{17}\ \mathrm{cm}^{-3}$ and 460 $\mathrm{cm}^2/\mathrm{V\,s}$, respectively. Note that the temperature of the laser-heated lattice at incident power of 0.25 mW (313 K) is only slightly higher than room temperature and hence the carrier concentration and mobility can be treated as room temperature values. The line shape analyses of lattice temperature dependent Raman spectra shed some light on the behavior of phonon and plasmon vibrations in NWs. The carrier concentration is fairly constant ($2.1-2.2\times10^{17}\ \mathrm{cm}^{-3}$) over the temperature range between 313 and 473 K. This behavior is consistent with data reported for bulk GaN samples of weak activation energy ($E_d=14$ meV).[32,33] The carrier concentration derived from an empirical formula described in Eq. (1) for room temperature is about $4\times10^{17}\ \mathrm{cm}^{-3}$. The accurate line shape analysis gives only about $2.2\times10^{17}\ \mathrm{cm}^{-3}$. The carrier concentration, mobility and plasmon frequency obtained by this line shape analysis are expected to be more accurate because the fitting includes all the parameters which influence the transport properties of carriers and mobilities. Figure 4 shows the electron mobility plotted as a function of laser induced temperature in comparison with data extracted from literature for GaN bulk[33] and NWs.[18] The linear decay of mobilities between 460 and 100 $\mathrm{cm}^2/\mathrm{V\,s}$ for 313 to 473 K shows that the LO phonon scattering becomes dominant in NWs, as do most of the bulk GaN samples. The rate of decay quite agrees with the reported temperature dependent electron mobilities of GaN compact layers.[32,33]

The line shape analysis model has also been extended to Si-doped GaN NWs for the determination of doping levels. Figure 5 shows the coupled LO phonon spectra of vertical aligned as-grown Si-doped and undoped GaN NWs for 3.65 mW laser excitation power. As a result of Si doping, the $L+$ mode is displayed at 749.3 cm^{-1}, thus shifted by 9.9 cm^{-1} as compared to undoped GaN NWs (739.4 cm^{-1}). The broad peak centered at 723 cm^{-1} is ascribed to the SO mode which is upshifted by 20 cm^{-1} as compared to undoped NWs. For the line shape analysis the influence of scattered SO phonon mode has been suppressed by extremely careful peak fitting.

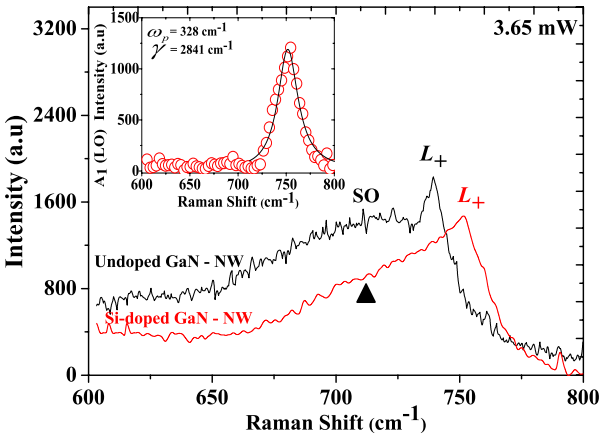

FIG. 5. (Color online) Micro-Raman spectra of vertically aligned undoped and doped GaN NWs recorded in backscattering geometry for excitation laser power of 3.65 mW. The inset shows a fitting curve for Si doped GaN NWs by line shape analysis.

The inset of Fig. 5 shows the comparison of the experimental and fitted line shape curve of the $L+$ mode for doped GaN NWs. By fitting, ω_p and γ are found to be 328 and 2841 cm^{-1}, respectively. The electron-plasmon damping (γ) is several folds stronger than that of undoped NWs (385 cm^{-1}). The line shape and frequency of the $L+$ mode can be correlated with an enhanced electron concentration due to Si-doping. The laser induced lattice temperature for the excitation power of 3.65 mW is about 470 K. The estimated donor concentration and mobility for the doped GaN NWs from Eqs. (7) and (8) are $n=1.3\times10^{18}$ cm^{-3} and $\mu=15$ cm^2/V s, respectively. As expected, Si-doping substantially increases the donor concentration of intentionally doped wires and decreases the electron mobility.

IV. SUMMARY

In summary, the line shape analysis of excitation power dependent μ-Raman scattering has been proven to be a noncontact versatile tool to measure the electrical, optical, and surface properties of free-standing GaN NWs. The electron concentration of strain free NWs at room temperature is about 2×10^{17} cm^{-3} and found to be insensitive to lattice heating. The estimated room temperature mobility is 460 cm^2/V s and found to decrease with temperature in agreement with published data for bulk GaN layers. The donor concentration and mobility for the doped GaN NWs are about 1×10^{18} cm^{-3} and 15 cm^2/V s, respectively.

ACKNOWLEDGMENTS

The authors K.J. and R.K.D. acknowledge the financial support from Alexander von Humboldt (AvH) foundation and Helmholtz-DAAD Fellowship, respectively. The authors wish to thank K. H. Deussen for technical support. We acknowledge Dr. D. Wang and Dr. M. Park, Auburn University, Alabama for their valuable advice on line shape analysis.

[1] E. D. Minot, F. Kelkensberg, M. van Kouwen, J. A. van Dam, L. P. Kouwenhoven, V. Zwiller, M. T. Borgstrom, O. Wunnicke, M. A. Verheijen, and E. P. A. M. Bakkers, Nano Lett. **7**, 367 (2007).
[2] Y. Huang, X. Duan, and C. M. Lieber, Small **1**, 142 (2005).
[3] O. Hayden, R. A. Agarwal, and C. M. Lieber, Nature Mater. **5**, 352 (2006).
[4] A. B. Greytak, C. J. Barrelet, Y. Li, and C. M. Lieber, Appl. Phys. Lett. **87**, 151103 (2005).
[5] J. C. Johnson, H.-J. Choi, K. P. Knutsen, R. D. Schaller, P. Yang, and R. J. Saykally, Nature Mater. **1**, 106 (2002).
[6] H. Kind, H. Yan, B. Messer, M. Law, and P. Yang, Adv. Mater. (Weinheim, Ger.) **14**, 158 (2002).
[7] K. Keem, H. Kim, G.-T. Kim, J. S. Lee, B. Min, K. Cho, M.-Y. Sung, and S. Kim, Appl. Phys. Lett. **84**, 4376 (2004).
[8] F. Patolsky, G. Zheng, and C. M. Lieber, Nanomedicine **1**, 51 (2006).
[9] F. Patolsky, G. F. Zheng, and C. M. Lieber, Anal. Chem. **78**, 4260 (2006).
[10] Y. Cui, Z. Zhong, D. Wang, W. U. Wang, and C. M. Lieber, Nano Lett. **3**, 149 (2003).
[11] Y. Huang, X. Duan, Y. Cui, and C. M. Lieber, Nano Lett. **2**, 101 (2002).
[12] R. Meijers, T. Richter, R. Calarco, T. Stoica, H. P. Bochem, M. Marso, and H. Lüth, J. Cryst. Growth **289**, 381 (2006).
[13] T. Kuykendall, P. J. Pauzauskie, Y. F. Zhang, J. Goldberger, D. Sirbuly, J. Denlinger, and P. D. Yang, Nature Mater. **3**, 524 (2004).
[14] E. A. Stach, P. J. Pauzauskie, T. Kuykendall, J. Goldberger, R. R. He, and P. D. Yang, Nano Lett. **3**, 867 (2003).
[15] X. Duan, J. Wang, and C. M. Lieber, Appl. Phys. Lett. **76**, 1116 (2000).
[16] R. Calarco, M. Marso, T. Richter, A. I. Aykanat, R. Meijers, A. v. d. Hart, T. Stoica, and H. Luth, Nano Lett. **5**, 981 (2005).
[17] A. Cavallini, L. Polenta, M. Rossi, T. Richter, M. Marso, R. Meijers, R. Calarco, and H. Lüth, Nano Lett. **6**, 1548 (2006).
[18] D. Wang, C. C. Tin, J. R. Williams, M. Park, Y. S. Park, C. M. Park, T. W. Kang, and W. C. Yang, Appl. Phys. Lett. **87**, 242105 (2005).
[19] T. Kozawa, T. Kachi, H. Kano, Y. Taga, M. Hashimoto, N. Koide, and K. Manabe, J. Appl. Phys. **75**, 1098 (1994).
[20] H. Harima, J. Phys.: Condens. Matter **14**, R967 (2002).
[21] M. V. Klein, B. N. Ganguly, and P. J. Colwell, Phys. Rev. B **6**, 2380 (1972).
[22] C. Wetzel, W. Walukiewicz, E. E. Haller, J. Ager, I. Grzegory, S. Porowski, and T. Suski, Phys. Rev. B **53**, 1322 (1996).
[23] H. Siegle, G. Kaczmarczyk, L. Filippidis, A. P. Litvinchuk, A. Hoffmann, and C. Thomsen, Phys. Rev. B **55**, 7000 (1997).
[24] H. Harima, J. Phys.: Condens. Matter **14**, R967 (2002).
[25] P. Perlin, C. Jauberthie-Carillon, J. P. Itie, A. S. Miguel, I. Grzegory, and A. Polian, Phys. Rev. B **45**, 83 (1992).
[26] V. Y. Davydov, Y. E. Kitaev, I. N. Goncharuk, A. N. Smirnov, J. Graul, O. Semchinova, D. Uffmann, M. B. Smirnov, A. P. Mirgorodsky, and R. A. Evarestov, Phys. Rev. B **58**, 12899 (1998).
[27] T. Azuhata, T. Sota, K. Suzuki, and S. Nakamura, J. Phys.: Condens. Matter **7**, L129 (1995).
[28] P. Perlin, J. Camassel, W. Knap, T. Taliercio, J. C. Chervin, T. Suski, I. Grzegory, and S. Porowski, Appl. Phys. Lett. **67**, 2524 (1995).
[29] V. V. Mamutin, V. A. Vekshin, V. N. Jmerik, V. V. Ratnikov, V. Y. Davydov, N. A. Cherkashin, S. V. Ivanov, G. Pozina, J. P. Bergman, and B. Monemar, IPAP Conf. Ser. **1**, 413 (2000).
[30] H. W. Lo and A. Compaan, Phys. Rev. Lett. **44**, 1604 (1980).
[31] G. Irmer, V. V. Toporov, B. H. Bairamov, and J. Monecke, Phys. Status Solidi B **119**, 595 (1983).
[32] W. Gotz, N. M. Johnson, C. Chen, H. Liu, C. Kuo, and W. Imler, Appl. Phys. Lett. **68**, 3144 (1996).
[33] X. Q. Shen, T. Ide, S. H. Cho, M. Shimizu, S. Hara, H. Okumura, S. Sonoda, and S. Shimizu, Proceedings of the International Workshop on Nitride Semiconductors [IPAP Conf. Ser. **1**, 162 (2000)].